Journal of Nuclear Materials 533 (2020) 152134

Contents lists available at ScienceDirect

Journal of Nuclear Materials

journal homepage: www.elsevier.com/locate/jnucmat

Evaporation of materials from the molten salt reactor fuel under elevated temperatures

Jarmo Kalilainen *, Sergii Nichenko , Jiri Krepel

Paul Scherrer Institute, CH-5232, Villigen, Switzerland

HIGHLIGHTS

- Novel simulation of Cs and I release from the MSR fuel in accident conditions.
- Mixing effects in the salt reduce fission product release.
- Mixing affects the speciation of evaporated fission products.

ARTICLE INFO

Article history:
Received 12 November 2019
Received in revised form
20 March 2020
Accepted 23 March 2020
Available online 24 March 2020

Keywords:
Molten salt reactor
Fission product release
Severe accident

ABSTRACT

The release of fission product and salt compounds from a molten salt reactor fuel under accident conditions was investigated with coupled computer simulations. The thermodynamic modeling of the salt and fission product mixture was performed in The Gibbs Energy Minimization Software GEMS and the obtained compound vapor pressures were exchanged with the severe accident code MELCOR, where the evaporation from a salt surface located at the bottom of a confinement building was simulated. The fuel salt considered in the simulations was LiF-ThF_4-UF_4 with fission products Cs and I. The composition of the fuel salt material was obtained from an equilibrium fuel cycle simulation of the salt using the EQL0D routine coupled to the Serpent 2 code. The results were compared to simulations using pure compound vapor pressures in the evaporation simulations. It was observed that by modeling the salt mixing the release of fission products and salt materials was reduced when compared to the pure compound simulations. The mixing effects in the salt, when compared to the pure compound simulation also affected evaporation temperatures and therefore the timing of the release of compounds. In an additional simulation in which the depressurization of the confinement was considered, the total evaporated mass of compounds increased due to increased mass transfer at the salt surface. The simulation process described in this paper can be used for a more comprehensive accident analysis of molten salt reactors once the detailed description of the reactor confinement and accident sequences are available and more fission product elements have been added to the analysis.

1. Introduction

Formation and transport of radioactive vapors and aerosol particles play a key role in the source term evaluation in severe nuclear accidents. In a typical Light Water Reactor (LWR), most of the Fission Products (FPs) transported in the Reactor Coolant System (RCS) will be in particulate form. Most notable non aerosol FPs are the noble gases Xe and Kr and iodine, which can form molecular I_2 or organic iodine compounds, which exist in vapor phase in the RCS or in the containment building. The behavior of FP compounds depends, for example, on the concentration of the different species and on the thermal-hydraulic conditions, like temperature and pressure, of the RCS and the containment. Most of today's severe accident analysis codes have been developed for LWRs. They feature, for example, models for the release of radioactive material from the degraded and molten LWR fuel, chemistry of volatile species and aerosol formation and transport. By simulating the mechanisms of the aerosol formation and their transport in the plant alongside the vapor phase species evolution, the source term in the containment structure can be estimated.

In a Molten Salt Reactor (MSR), the fuel can be dissolved in the salt that also acts as the reactor coolant. One of the MSR designs is

* Corresponding author.
E-mail address: jarmo.kalilainen@psi.ch (J. Kalilainen).

https://doi.org/10.1016/j.jnucmat.2020.152134

Abbreviations and symbols

FP	Fission Product
LWR	Light Water Reactor
MSR	Molten Salt Reactor
MSFR	Molten Salt Fast Reactor
EFPY	Effective Full Power Year
RCS	Reactor Coolant System
TDB	ThermoDynamic Database
VP	Vapor Pressure
m	Mass (kg)
C	concentration (kg/m^3)
t	time (s)
A	Surface area (m^2)
k	mass transfer coefficient (m/s)
P	pressure (Pa)
M	molar mass (mol/kg)
T	temperature (K)
R	Ideal gas constant J/(K·mol)
D	diffusivity (m^2/s)
Sh	Sherwood number
Nu	Nusselt number
Pr	Prandtl number
Sc	Schmidt number
Ω	collision integral
G^{EX}	Excess Gibbs energy J/mol

the Molten Salt Fast Reactor (MSFR), which features a fast neutron spectrum, operation in the thorium cycle [1] and uses LiF-ThF_4-UF_4 (77.5-20-2.5 mol%) as a fuel salt. Because of its completely different design principles compared to LWRs, the release of radioactive material in an accident condition would look fundamentally different in the MSR compared to an LWR. In a typical LWR, the FPs and actinides are released from the fuel rods to the surrounding coolant after the cladding failure. Integral severe accident simulation codes typically use semi-empirical models such as the CORSOR models in MELCOR [2] or ELSA module in ASTEC [3] to model radionuclide release during the core degradation. In an MSR however, the accident conditions could lead to a heat-up of the core and release of radioactive materials by evaporation from the already liquid molten salt fuel. After being released from the molten salt, the vapor phase materials can condense to form aerosols whose transport in the fuel circuit and in the confinement will contribute to the radioactive source term.

The most extensive experimental studies on fission product migration in an MSR were conducted during the Molten Salt Reactor Experiment (MSRE) at the Oak Ridge National Laboratory [4]. Several tests on FP behavior in MSRE were performed during the reactor operation. The samples were collected from the pump bowl salt and gas. The main conclusions of the investigators were that FPs Rb, Cs, Sr, Ba, the lanthanides and Y and Zr remain soluble in the salt. However, from the above mentioned elements, ^{89}Sr and ^{137}Cs isotopes are formed through noble gas precursors ^{89}Kr and ^{137}Xe, which are insoluble in the salt. The study indicated that these materials existed also outside the fuel. Additionally, the salt sampling in the MSRE indicated that 45–71% of the ^{131}I was not contained in the fuel salt. Also only 1% of the ^{131}I was found in the gas samples, leaving a significant amount of iodine unaccounted for. Additionally, Nb, Mo, Tc, Ru, Ag, Sb and Te were found insoluble in the fuel salt with most of them deposited (plated out) on the metal or graphite surfaces and only 1–20% of them remained in the salt. For more details, please refer to Ref. [4].

After MSRE, investigations on the FP behavior in MSRs have been scarce. Related to the MSFR, several experimental and analytical studies have been performed to determine the thermodynamic properties of the fuel salt with Cs and I additives [5–7]. They concentrate mainly on the species cesium fluoride (CsF) and cesium iodide (CsI), which are considered as the most stable forms of these FPs in the MSR fuel [7]. These investigations show that Cs is retained in the molten salt as CsF, but CsI solubility in a LiF–ThF_4 salt is limited. Additionally, evaporation of Cs and I from FLiNaK salt has been recently studied. Taira et al. [8] studied the evaporation of Cs and I using mass spectrometry and concluded that CsI is retained by the salt with CsI/FLiNaK mixtures 1–100 mol. With larger CsI concentrations (CsI/FLiNaK mixture more than 10%), CsI may not be fully dissolved in a temperature range 823 K–11173 K used in the experiments. Furthermore, gas phase KI formation was observed indicating a reaction between the fuel salt and CsI to form new iodine compound. Sekiguchi et al. [9] measured vapor pressures of salt compounds Cs and I using different CsI, CsF to FliNaK salt ratios. They concluded that CsI was not well retained in the salt whereas CsF activity coefficients indicated better retention [9]. CsI is considered to be one of the most important species transporting iodine in the conditions of LWR severe accident [10]. Its volatility in the molten salt, indicated by the experiments described above, requires its consideration also in the MSR accident analysis.

In this study, the volatility of the MSFR fuel and FP species in accident conditions was evaluated by coupling two simulation tools: the MELCOR 2.2 severe accident code and the GEMS thermodynamic modeling package. A simplified model of an accident condition, where the fuel salt is drained from the fuel casing onto the floor of a confinement with nitrogen atmosphere was created, and release of fission product and salt material from the surface of a molten salt pool was modeled. MELCOR was used to model the evaporation process and the thermal-hydraulic conditions in the confinement and GEMS for obtaining the salt/FP speciation. For accurate thermodynamic simulations, a model of the mixed salt/FP liquid was created with GEMS and validated against the available literature data. The FP elements considered in this study were Cs and I, and the initial concentration of fission product and salt species was obtained from the simulations of the equilibrium fuel cycle of the MSFR. The description of FP chemistry in the standalone MELCOR code is limited. For example, condensation/evaporation processes are modeled using predetermined list of equilibrium vapor pressures. To investigate the validity of this simplified approach in MSRs, the results obtained with the coupled MELCOR/GEMS will be compared to standalone MELCOR simulations using pure compound vapor pressures for the evaporating species, obtained from the literature. As a sensitivity analysis, additional simulations using different thermal-hydraulic boundary conditions in the confinement were performed.

To the best of the authors' knowledge, the work presented in this paper is the first attempt towards a more realistic modeling of the radionuclide release from the MSR under severe accident conditions. Not many details exist on the design and geometry of the MSFR containment/confinement building. Geometry for a decay heat removal system in MSR was suggested by Wang et al. [11] and the design of the MSFR confinement barriers was presented at the conclusion of the EU SAMOFAR project [12]. The confinement volume, overall geometry and the initial and boundary conditions of the model will have an effect on the activity release and transport modeling. In this work however, our focus was to develop a release model for the MSR fuel that takes into

account the salt chemistry and its effects on the salt and FP volatility. Thus, once the more detailed information of the confinement building and the accident sequence will be available, the release model described in this paper can be applied for a more detailed analysis of the radionuclide transport and source term evolution in MSR accidents.

2. Methods and tools

The following sections describe the simulation tools and models used in this study. Brief introduction of MELCOR, GEMS and EQL0D codes is provided and the MSR confinement evaporation model along with the thermodynamic modeling of the salt are described.

2.1. Fission product composition in MSFR fuel: EQL0D routine

The EQL0D routine [13,14] was applied to simulate the equilibrium isotropic fuel salt composition in MSFR and to obtain the initial salt composition for the evaporation simulations. The routine was initially designed for equilibrium fuel cycle calculations but it is also capable of simulating fuel evolution over a finite number of steps, similar to a standard depletion code.

EQpL0D uses two loops:

1. an outer loop in which Serpent 2 [15] is called and the burn-up matrices for the system are created, and
2. an inner loop in which the system is solved and batch-wise processes (refueling operations, redox and criticality control) are performed.

The role of the outer loop is to update cross-section and neutron flux data; the inner loop depletes materials and refuels them. In the equilibrium mode, the inner and outer loops are executed until the selected convergence criteria are fulfilled and equilibrium is reached. As a typical criterion, the changes of selected actinide isotope concentration need to be below 10^{-5} or 10^{-6} of the relative concentration. In the general mode, each loop is ran several times according to user input.

Depletion matrices for burnable materials and analog reaction rates for criticality search are obtained from Serpent 2. Fuel processing matrices are created to include continuous addition or removal coefficients. To solve the Bateman equations, EQL0D uses the Chebyshev Rational Approximation Method (CRAM) [16], implemented in MATLAB in a manner similar to that of Serpent.

MSFR is designed as an internal breeder where the majority of the fuel is bred within the fuel salt via neutron activation of ^{232}Th to yield ^{233}U. Nonetheless, it utilizes a blanket salt to increase the neutron economy and breeding performance. The simplified fuel cycle scheme can be seen in Fig. 1.

In the simulations, the fuel salt of MSFR was reprocessed using a batch-wise extraction and reprocessing rate of 40 l per day. The blanket treatment was simplified, volatile fission products were continuously removed, U/Np/Pu extracted to fuel and soluble fission products were not removed from the blanket salt. The fuel salt was cooled for 2 days before the reprocessing stage was initiated.

The daily removal of 40 l of salt corresponds to complete salt loading processing in 450 days. This is called effective cycle time. The effective cycle time for gases He, Ne, Ar, Rn, Kr, Xe and elements Ru, Rh, Pd, Ag, Nb, Mo Tc, Sb, Te was only 43 s. These properties have been adopted from the MSFR core specifications [17]. The composition of fission products dissolved in the fuel salt was enumerated after 200 EFPY operation of the MSFR. The fission products remaining in the salt at the equilibrium are shown in Fig. 2, which highlights elements Cs and I whose evaporation behavior was considered in this study.

The amount of I and Cs in the fuel salt is relatively low. Since elements Sb and Te, which decay to I, are removed from the core by the off-gas system with a cycle time of 43 s, the majority of I originates in the off-gas system. The same statement is also valid for Cs, as its precursors Te and Xe are also removed via the off-gas system. The iodine isotopes with substantial individual fission yield are isotopes 133, 124, 135, 136, and 137 and they all decay relatively fast to Xe. The known problematic isotope of ^{137}Cs has direct fission yield less than 1% and the cumulative yield is more than 6%. Accordingly, 80% of ^{137}Cs originates from Xe decay.

The rapid removal of the FPs described above will strongly depend on the salt properties. According to the redox potential, the metallic FPs can also form fluorides. Nonetheless, the burnup simulation was not coupled to the thermodynamics simulation and it was assumed that the reactor is only operated at nominal redox potential. This is foreseen for the future studies. So far, only the liquidus temperature has been evaluated based on burnup calculations [18].

2.2. Salt evaporation: MELCOR 2.2 code

MELCOR is a lumped parameter computer code used mainly for severe accident simulations in the LWRs. Capabilities for modeling advanced reactors and other systems like high temperature gas-cooled reactors and spent fuel pools have been later added to the code. Detailed description of the MELCOR code can be found from the reference manual [2]. Even though the molten salt reactor is not part of the designs currently included in MELCOR, the flexibility of the code allows the user to simulate different physical phenomena independent of the reactor design, relevant also for the MSR. In this work, MELCOR 2.2 code was used to simulate vaporization of user defined salt and fission product species in a geometry representing

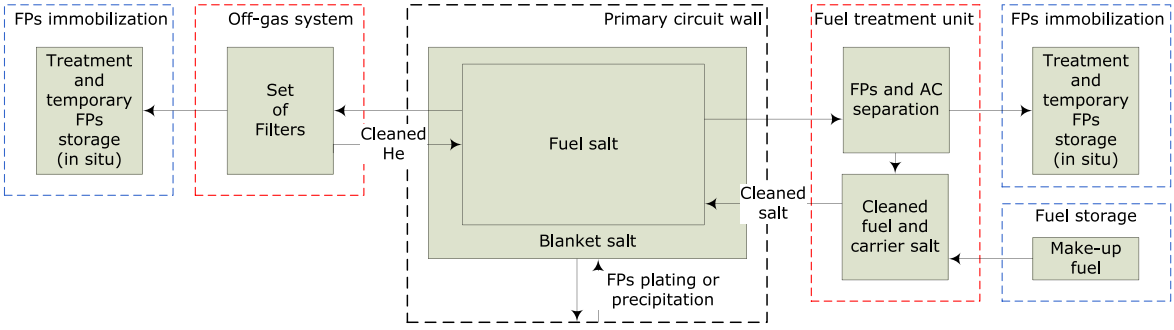

Fig. 1. Simplified MSFR fuel cycle.

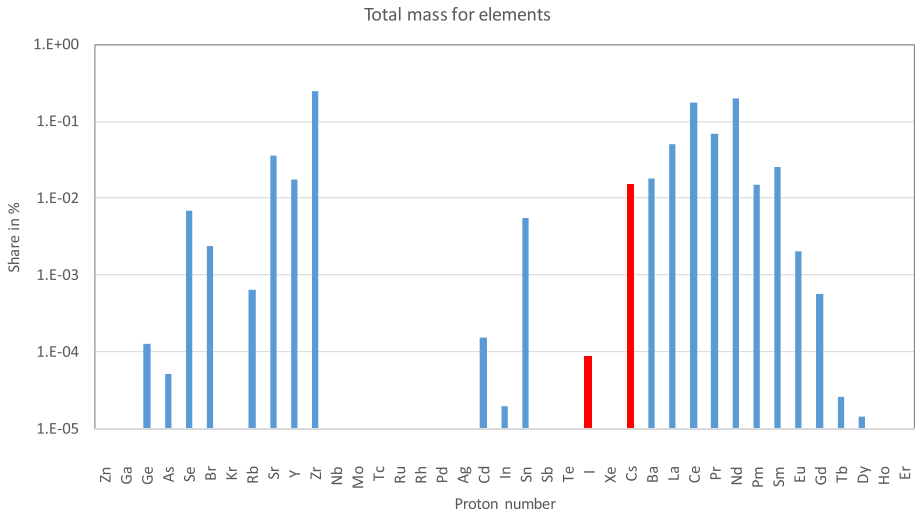

Fig. 2. Detailed distribution of fission products in the fuel salt.

the preliminary design of a confinement building of a molten salt reactor.

2.2.1. Evaporation modeling

In MELCOR, the condensation and evaporation of radionuclides to and from heat structure surfaces or onto surfaces of aerosol particles is determined by a set of equations based on the TRAP-MELT2 model [2]. A standard MELCOR input does not allow user to define an initial condensed radionuclide mass onto a heat structure surface. Thus, in order to use the code to simulate a source of evaporating vapors from the molten salt, the model described below was embedded to the MELCOR input with user defined control functions.

Equation (1) describes the evaporation of mass dm_i of a compound i from the salt surface to the neighboring control volume. In Eq. (1), A is the area of the surface where the evaporation is taking place (here the surface area of the control volume floor), k_i is the mass transfer coefficient and C_i^a is the concentration of the species i in the control volume atmosphere neighboring the surface.

$$\frac{dm_i}{dt} = Ak_i(C_i^s - C_i^a) \tag{1}$$

The model assumes equilibrium between the salt and the gas atmosphere near the salt surface, where the concentration of the evaporating species depends on the saturation concentration C^s.

$$C^s = \frac{P_i^s(T)M_i}{RT} \tag{2}$$

In Eq. (2), C^s is determined by the saturation vapor pressure $P_i^S(T)$ of the species, M_i is the molecular weight of compound i, R is the ideal gas constant and T is the temperature of the control volume atmosphere. When the saturation concentration of a vapor species i exceeds its current concentration in the control volume atmosphere, evaporation of i from the surface will take place at a rate defined by Eq. (1). The model assumes the direct proportionality between the mass transfer coefficient k and the diffusivity D, which originates from the so called "film theory", used in the simplified mass transfer simulations [19]:

$$\frac{k_i}{k_{st}} = \frac{D_{i,N_2}}{D_{st,a}} \tag{3}$$

$D_{i,N2}$ is the binary diffusivity of evaporating compound i in N_2, k_{st} is the mass transfer coefficient of steam and the diffusivity of steam in the air atmosphere $D_{st,a}$ is defined as [2]:

$$D_{st,a} = 4.7931 \times 10^{-5}\frac{T^{1.9}}{P^a} \tag{4}$$

The mass transfer coefficient of steam k_{st}, is calculated by the MELCOR code during each calculation time step:

$$k_{st} = \mathrm{Sh}\frac{D_{st,a}}{L_c} \tag{5}$$

The Sherwood number Sh in Eq. (5) is obtained in MELCOR using the correlation:

$$\mathrm{Sh} = \mathrm{NuSc}^{1/3}\mathrm{Pr}^{1/3} \tag{6}$$

Nu, Sc and Pr are the Nusselt, Schmidt and Prandtl numbers, respectively. In this work, the confinement atmosphere is considered initially to consist of only pure nitrogen as a noncondensable gas. The binary diffusivity of evaporating compound i in N_2 can be calculated using [2]:

$$D_{i,N_2} = 0.0018583\frac{T^{3/2}\sqrt{M_i^{-1} + M_{N_2}^{-1}}}{P\sigma_{iN_2}^2\Omega_{D,iN_2}} \tag{7}$$

For the collision integral of a binary system Ω_{D,iN_2}, the following curve fit was obtained from Bird et al. [20]:

$$\Omega_{D,iN_2} = \frac{1.06036}{T^{0.15610}} + \frac{0.19300}{exp(0.47635T^*)} + \frac{1.03587}{exp(1.52996T^*)} + \frac{1.76474}{exp(3.89411T^*)}, T^* = \frac{kT}{\varepsilon_{iN_2}} \tag{8}$$

The Lennard-Jones parameters for a binary system σ_{iN_2} and ε_{iN_2} were calculated using:

$$\sigma_{iN_2} = 0.5(\sigma_i + \sigma_{N_2}), \varepsilon_{iN_2} = \sqrt{\varepsilon_i \varepsilon_{N_2}} \quad (9)$$

where MELCOR 2.2 default values were used for the Lennard-Jones parameters of fission products and salt components, which are [2]: σ_i = 3.617Å, $\frac{\varepsilon_i}{k}$ = 97.0 K and for nitrogen: σ_{N_2} = 3.798Å and $\frac{\varepsilon_{N_2}}{k}$ = 71.4 K.

Using the above information, the mass transfer coefficient k_i for any evaporating species is obtained from Eq. (3).

Finally, the saturation vapor pressure used in Eq. (2) of compound i is introduced to the MELCOR code as a function of temperature described in Eq. (10). The coefficients will be obtained either using GEMS in the coupled simulations or from literature values. This process will be described in the following sections.

$$\log_{10} P_i^s = A + B/T + C\log_{10} T \quad (10)$$

During the evaporation simulation, MELCOR will keep track of the elemental composition of the salt, which will be needed as an input for the thermodynamic simulations. The initial composition of the salt was obtained from the EQL0D simulations described above.

2.2.2. Simulation model for MSR confinement

Fig. 3 shows a schematic of the geometry used in the MELCOR simulations. The confinement is modeled as a cylindrical container with a salt layer at the bottom surface. In the middle of the confinement is a fuel casing, from which the salt has been in accident conditions drained uniformly distributed at the bottom of the confinement. A gas-gas heat exchanger is encircling the confinement at 15 m above the floor level. The heat exchanger surface area is approximately 235 m^2. The initial confinement atmosphere consists of nitrogen gas at 0.1 MPa pressure.

As shown in Fig. 3, the MELCOR model of the confinement is divided into 14 control volumes (CVs) which are connected with flow paths allowing convective heat transfer and transport of the evaporated materials. Adiabatic temperature boundary conditions are set to all confinement boundary heat structures, except on the isothermal heat exchanger and salt surfaces. The hot salt and the colder heat exchanger induce natural convective flow in the container, driving the heat and mass transfer. Along with convection, also heat conduction and thermal radiation are considered in the MELCOR simulation. Due to a lack of data on the emissivity of the MSFR salt, a value of 0.44 [21], measured for sodium sulfate was used in the simulations.

The salt layer at the bottom of the confinement is also described by a heat structure. At simulation time t = 0 s, the salt surface heating was started at a rate 6 K/min, simulating the salt heat-up due to the decay heat. The initial temperature of the salt, all confinement surfaces and the atmosphere was set to 300 K. Low initial salt temperature was chosen for this study so that the thermodynamic behavior of the fuel salt could be investigated in a broad range of temperatures (300 K–1500 K). In addition, the slow heating rate allowed the changes of the evaporation process in different fuel temperatures to be clearly observed. The heat exchanger temperature was increased from 300 K with a heating rate similar to the salt until it reached the temperature 500 K after which it was kept constant. At each simulation time step, the evaporated rate of FPs and salt components from the salt surface to the bottom CVs 1–3 is calculated using Eq. (1).

Additionally, we investigated the effect of a rapid confinement depressurization on the salt evaporation, which could be performed as an accident management measure or could be due to a failure of the pressure boundary. The confinement was depressurized through an orifice with a diameter of 0.1 m and approximately 70 cm^2 surface area in CV14 once the confinement pressure rose above 0.2 MPa (abs). The results from the depressurization simulation were compared with the reference simulation.

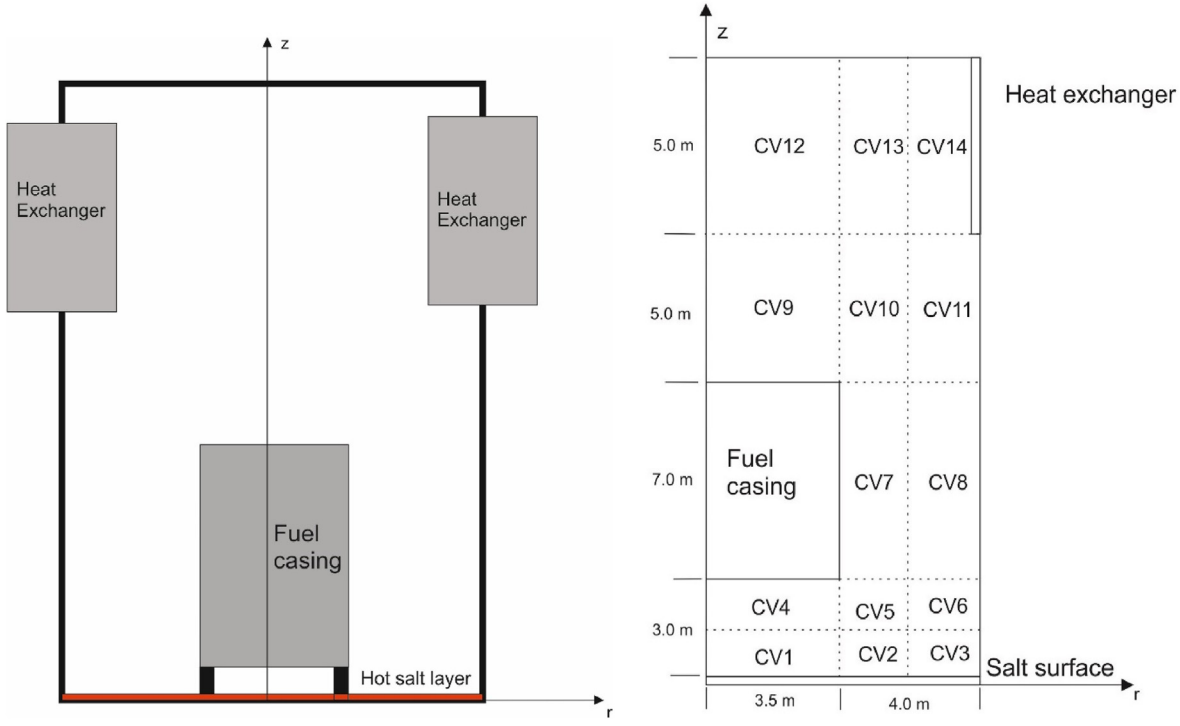

Fig. 3. The schematic of the axisymmetric model of the simulated confinement.

2.3. Thermodynamics of the salt: GEMS and Heracles database

The Gibbs Energy Minimization Software for Thermodynamic Modeling (GEMS TM) has been developed over 17 years at the Paul Scherrer Institut (PSI). GEMS codes [22], in part open-source, are widely used in various fields of application, including cement chemistry, radioactive waste disposal, and nuclear energy research. GEMS TM includes the GEMSFITS code [23], which is an advanced tool for model parameter optimization and improvement of internal consistency of thermodynamic databases against experimental data.

A critical issue of any thermodynamic model, independently of the code used, is the quality and completeness of the underlying thermodynamic database. Because the results of thermodynamic calculations cannot be better than the input data on which they rely, one of the core activities for GEMS development has been the implementation of high-quality databases. Hence, for applications to nuclear materials and spent-fuel reprocessing, the HERACLES ThermoDynamic Database (TDB) for low pressure - high temperature non-aqueous systems has been developed and maintained at PSI since 2010 [24]. HERACLES TDB covers molar thermodynamic properties of solid, liquid (melt) and gaseous (plasma) compounds of actinides, fission products, and minor actinides. It is valid up to at least 3000 K, covering the majority of the elements of interest. At temperatures above 3000 K reliable experimental data on thermodynamic properties of different species is scarce and of questionable quality.

2.3.1. LiF–ThF_4–UF_4–Cs–I system modeling in GEMS

The thermodynamic database HERACLES has been extended with the newly obtained information on binary interaction parameters for various systems. It should be noted that interaction parameters of higher orders (ternary etc.) are not considered in this work but could be included in the HERACLES DB if needed. Information on excess Gibbs energy for binary systems together with the information on thermophysical properties of pure compounds was used to study the speciation and the volatilities of different salt and fission product species in the MSR fuel melts. In the previous work [25], the GEMS package was applied for the parameterization of excess Gibbs energy functions of different binary fluoride and iodide systems (e.g. LiF–ThF_4, ThF_4–CsF, CsF–CsI). For this purpose, the Redlich-Kister (Guggenheim) mixing model was used. The model is based on Guggenheim's expansion series for the excess Gibbs energy of mixing [26]:

$$G_{ij}^{EX} = RTx_ix_j\left[a_0 + a_1(x_i - x_j) + a_2(x_i - x_j)^2 + \ldots\right], \quad (11)$$

where a_0, a_1, a_n are dimensionless fitting parameters.

The interaction parameters were fit to reproduce excess enthalpies and phase equilibria information (liquidus and solidus temperatures) published by Capelli et al. [7,27]. In these publications, the information on the excess interactions for binary mixtures is given in the form of empirical parameters for the modified quasi-chemical model proposed by Pelton et al. [28]. At the time of this work, the Pelton model was not implemented in the GEMS thermodynamic package and, therefore, the published parameters were refitted (mapped) to the parameters of the Redlich-Kister model, available in GEMS. The first two-three terms in the Redlich-Kister model are generally sufficient to represent experimental data and are shown in Table 1. The information on binary excess interaction parameters allows for a modeling of multicomponent mixtures under the assumption that the multi-species (ternary and higher orders) interactions are negligible and the binary interactions are the dominant ones. Vapor pressures for different species of the LiF–ThF_4–CsF mixture calculated using the parameters from the Table 1 are presented in Fig. 4 together with the literature [7] (experimental and calculated) results. As can be seen from the Fig. 4, the interaction parameters presented in Table 1 reproduce the literature data correctly. The slight difference between the calculated results with GEMS and calculated results presented in the work of Capelli et al. [7] are attributed to different model used in this work.

The binary interaction parameters were used on the modeling of multicomponent mixtures with a consideration of the mixing effects in the solid and liquid phases. Mixing effects in the liquid phase lead to the deviation of the mixture/solution behavior from the ideal one. These deviations manifest themselves in the form of the reduced or increased melting temperatures compared to the ideal, appearance of the miscibility regions and changes to the components vapor pressures. In case of the molten salts, the excess Gibbs energies are negative which leads to a drop of the melting temperatures compared to the ideal behavior and to a reduction of the vapor pressures of the components of the melt. This in turn leads to the retention of the relevant compounds in the molten salt pool. The latter was studied in this work and the influence of the mixing effects on the salt evaporation was demonstrated.

Table 1
Interaction parameters for different binary systems of interest, obtained from the data in the references.

Pair	a_0	a_1	a_2	Reference data
LiF–ThF_4	−22105	−22951	−7122	[7]
LiF–CsF	−16000	0	0	[7]
CsI–LiI	−21478	4557	−2607	[7]
CsI–CsF	−2842.8	0	0	[7]
LiF–LiI	−650	1036	338	[7]
ThF_4–ThI_4	−62000	0	0	[7]
LiI–ThI_4	−22105	−22951	−7122	[7]
LiF-UF_4	−30046	−31196	−9681	[29]
CsF–ThF_4	−145000	0	0	[7]
CsI–ThI_4	−19575	5763	4090	[7]

2.4. GEMS-MELCOR coupling: cGEMS

The coupling between MELCOR and GEMS was done using

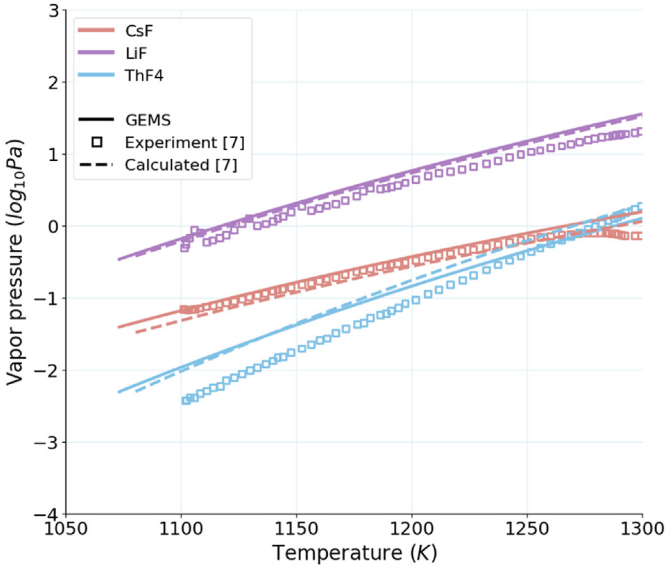

Fig. 4. Vapor pressure data for the LiF–ThF_4–CsF (75.73-23.23-1.05) mixture, calculated with GEMS and literature (experimental and calculated) [7].

cGEMS (coupled GEMS) code, developed at PSI to improve the chemical modeling in MELCOR in severe accident conditions. cGEMS serves as an interface between GEMS and MELCOR and can call both MELCOR and GEMS depending on the situation, and in this way has a controlling function in the simulation process. At the same time, cGEMS has direct access to the GEMS code through its API (Application Programming Interface) and can perform the data exchange between both codes. This simplified coupling allows for a step-wise modeling of a severe accident scenario using MELCOR and GEMS. In this study, "step-wise modeling" means that cGEMS runs the simulation in cycles following the path:

1) Run severe accident simulation in MELCOR for 200 s.
2) Collect data from the MELCOR, containing elemental composition and temperature of the salt and pass it to GEMS for thermodynamic calculations.
3) Run GEMS thermodynamic simulation.
4) Collect and prepare GEMS results: coefficients from the vapor pressure data for different species considered in the evaporation simulation and pass it to MELCOR using a new input file.
5) Repeat the cycle.

In the present work, during the preliminary simulations several different time steps (from 10 s up to 500 s) were tested. No noticeable difference was observed in the evaporated masses within this time step range. Therefore, in this work the 200 s time step was chosen under the assumption that the salt temperature does not vary much within this time step and therefore there will be no noticeable effect on the obtained modeling results.

The information on the vapor pressure of different species is passed to MELCOR in the form of the coefficients A, B and C of Eq. (10). By keeping the MELCOR simulation time relatively small (200 s in this study), the vapor pressures can be passed as constant values using only the "A" coefficients. Additionally, constant exchange of the information between MELCOR and GEMS ensures that calculated vapor pressures of different species accounts for the composition evolution of the molten salt pool due to evaporation. It should be noted that all the simulations have been done under the assumption that the total pressure in the system is kept at 0.1 MPa. This assumption implies that there is no noticeable effect of the total pressure on the thermodynamic properties of the compounds and mixing properties in the phases. This assumption is fair if the total pressure of the system does not vary much and the pressure effect become usually noticeable at pressures from MPa to GPa ([30–32]) that are much higher than confinement pressure during the transient in the MSR in this simulation, which is close to 0.1–0.5 MPa. Additionally, it needs to be noted that the thermodynamic simulations apply in equilibrium conditions, which are assumed to take place in a gas layer close to the salt surface, described in section 2.2.1. Also, the addition of other FP materials to the thermodynamic simulation could alter the equilibrium composition, thus increasing the uncertainty when applying the results presented in this paper to a more realistic salt composition.

3. Results and discussion

3.1. Vapor pressure of compounds in the salt mixture

The volatile compounds, which are to be considered in the evaporation simulations, were determined by modeling the LiF–ThF_4–UF_4–Cs–I system with GEMS. The concentrations of Li, Th, U, Cs and I was obtained from the EQL0D equilibrium simulation of the MSFR, described above. The amount of fluorine in the simulation was set to match a stoichiometry of fuel salt, i.e. all salt elements were represented in the simulation as LiF-ThF_4-UF_4 and the composition is shown in Table 2. The vapor pressures of gas phase compounds were determined at temperatures 300–1500 K and all species reaching vapor pressure above 10^{-8} Pa were chosen for the evaporation simulations. The vapor pressures of these species are shown in Fig. 5 and listed in Table 2.

Due to the concerns about corrosion of the structural materials by the molten salt, the control of the redox potential is important in MSRs. In the case of fluorides based MSR, the redox potential is typically monitored and controlled via the UF_4/UF_3 ratio, which varies with the operating time due to the fission reaction. It is also important to note that the volatility of the FP species can be significantly affected by the concentration of fluorine in the salt mixture. In these simulations, the set stoichiometric amount of fluorine leads to the UF_4/UF_3 ratio of about 431.0. In addition, the simulations showed that this ratio does not depend on the temperature within the studied temperature range (up to 1500 K). A sensitivity study, where the amount of F in the salt was either increased or decreased by 2% from the stoichiometric value was also performed, in order to investigate its effects on the speciation of FP elements like iodine. It allowed the covering of the UF_4/UF_3 ratio range from as low as 0.28 up to 10′000. In Fig. 6, I and I_2 vapor pressures with different levels of fluorination are depicted, showing how the extra F in the system hinders the formation of CsI leaving most of the I free to form molecular iodine in the salt. The figure also shows that the free iodine exists as I_2 at low temperatures (below ~800 K) and decomposes to I atoms once the temperature is increased. The study of the F amount effects on the redox behavior of the salt is out of the scope of this work due to its complexity and is a matter of future research.

3.2. Pure compound vapor pressures

In order to determine the effects of mixing in the evaporation of a fuel salt and fission products, evaporation simulations were also performed using saturation vapor pressures of the pure compounds, where no mixing effects are considered and no thermodynamic simulations were performed. In these simulations, the coefficients A, B and C in Eq. (10) were obtained using the available literature data and boiling point estimates for the species listed in Table 2. Obtained coefficient are shown in Table 3 and the curve fit for the pure compound vapor pressure of LiF is shown Fig. 7. No vapor pressure data was found for ThF_3(g) or I(g). Concerning iodine, the pure compound vapor pressure of molecular I_2 is very high compared to any of the species listed in Table 2 due to its low boiling point. In low temperatures, iodine will first evaporate as I_2 and once the temperature is increased, it decomposes to I. This behavior is similar to that observed also in the GEMS simulation in Fig. 6 with excess fluorine. In this work, the evaporation simulations were performed also in low salt temperatures (below 500 K). In the pure compound VP simulations, all iodine will be released from the salt before the decomposition of iodine to its atomic form takes place (see Fig. 6). Thus, only the evaporation of I_2 from the salt was taken into account in the pure compound simulations.

3.3. Simulation matrix for the evaporation simulations

Based on the preliminary thermodynamic simulation described in the previous section, the simulation matrix was prepared for the evaporation simulations and is shown in Table 4. All evaporation simulations use the Li, Th, U, Cs, I composition in the equilibrium salt, obtained from EQL0D simulation as an initial salt composition with the amount of fluorine matched for the stoichiometric composition of LiF, ThF_4 and UF_4, shown in Table 2. The different simulation cases are described in detail below and summarized in Table 4.

Table 2
Initial composition of the MSFR salt and the species considered in the evaporation simulations.

Initial composition in the salt	
LiF (mol%)	78.8
ThF_4 (mol%)	16.9
UF_4 (mol%)	4.2
Cs (mol%)	9.8e-3
I (mol%)	5.8e-5
Li (kg)	4720.0
Th (kg)	33910.0
U (kg)	8650.0
F (kg)	26787.0
Cs (kg)	11.0
I (kg)	0.06
List of species considered in the coupled evaporation simulations	
Salt species	Fission product species
Li, LiF, Li_2F_2, Li_3F_3, UF_3, UF_4, ThF_4,	I, CsI, CsF and LiI

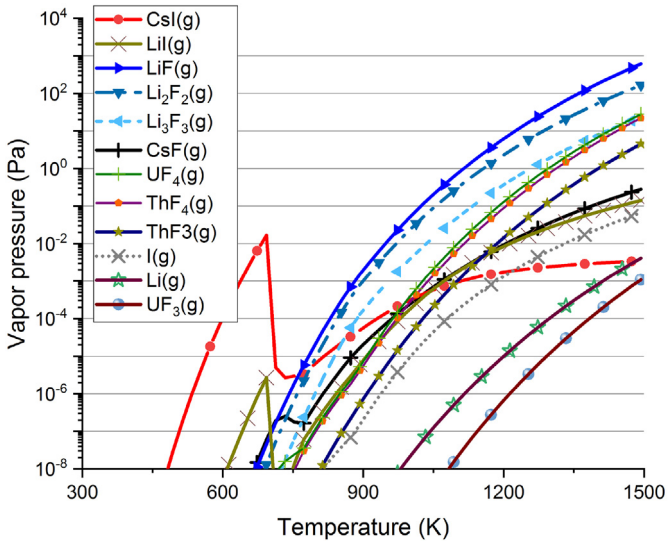

Fig. 5. Vapor pressures of the gas phase species chosen for the evaporation simulation.

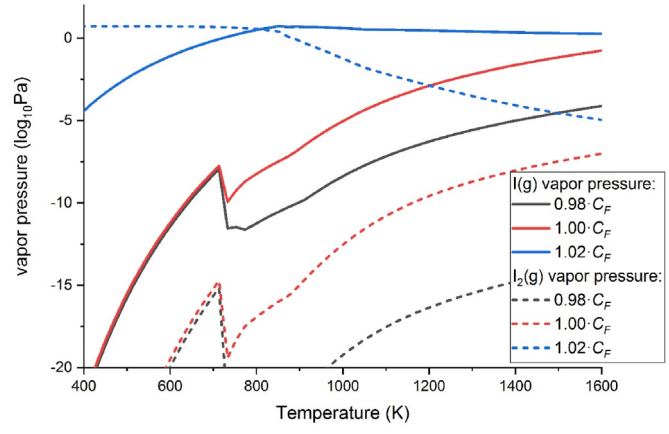

Fig. 6. Vapor pressures of I and I_2 with different fluorine concentration (C_F) in the salt mixture.

1. Case 1 represents the best estimate simulation, where GEMS was used to determine the salt mixture vapor pressures during the evaporation calculation.
2. In case 2, only MELCOR simulation was performed and the effects of the salt mixing on the evaporation behavior of the FPs and salt compounds was not considered. This simulation used the pure compound vapor pressures, obtained from the literature and listed in Table 3.
3. Case 3 was identical to case 2 with molecular iodine I_2 added to the list of evaporating species. It was performed in order to observe what effect the change in the iodine speciation will have on the simplified pure compound vapor pressure simulation. Both cases 2 and 3 will also signify the importance that the user choices of the speciation have on the behavior of the FPs and salt products if the thermodynamic simulations are not performed as a part of the evaporation modeling.
4. Finally, in case 4, depressurization of the confinement was considered. It uses the coupled simulation method to obtain the evaporating species VPs with the added venting when the confinement pressure increases up to 0.2 MPa (describes in section 2.2.2).

3.4. Results from the thermal-hydraulic simulation in MELCOR

Thermal-hydraulic parameters that have the largest effect on the MSR salt evaporation model presented in this study are pressure, atmospheric and salt temperature and the mass transfer coefficient at the salt surface. The temperature evolution of the salt as well as the gas atmosphere at different confinement elevations is shown in Fig. 8. It shows that there is very little stratification in the confinement atmosphere due to the mixing caused by the natural convective flow induced by the temperature difference between the hot salt surface and the cooler heat exchanger leading to approximately even gas temperature. Fig. 9 shows the evolution of the mass transfer coefficient of steam computed in the MELCOR code (Eq. (5)). It can be seen that in case 1, k_{st} behavior is very similar above all salt segments of the bottom control volumes 1–3. During the heat up of the salt, the flow conditions on top of the salt surface change, which causes the changes to k_{st} due to its dependence on the Sherwood number and steam diffusivity (Eqs. (5) and (6)). As the temperature of the gas atmosphere stabilizes at approximately t = 15000 s, k_{st} reaches a constant value of approximately 0.0037 m/s. The effect of depressurization to the mass transfer coefficient will be discussed more in the following

Table 3
List of coefficients used to calculate the vapor pressure of pure compounds.

	Constants			Reference data used for the fit	
	A	B	C	Vapor pressures	Boiling point
Li	13.927	−8411.918	−1.157	[33]	[33]
LiF	39.233	−17512.525	−7.673	[6,34,35]	[36]
Li_2F_2	11.969	−12863.330	0.0	[6,34]	Estimated with GEMS
Li_3F_3	11.695	−12734.668	0.0	[6,34]	Estimated with GEMS
UF_3	12.340	−16614.284	0.0	[37,38]	Estimated with GEMS
UF_4	99.511	−28515.009	−24.050	[39–41]	[42]
ThF_4	12.931	−15448.733	0.0	[5,6,43–45]	[42]
CsI	41.755	−12406.991	−9.013	[2,46]	[47]
CsF	10.820	−8861.135	0.0	[48–50]	[47]
LiI	27.581	−10989.817	−4.747	[51]	[36]
I_2	62.522	−5595.471	−17.022	[2,52]	[36]

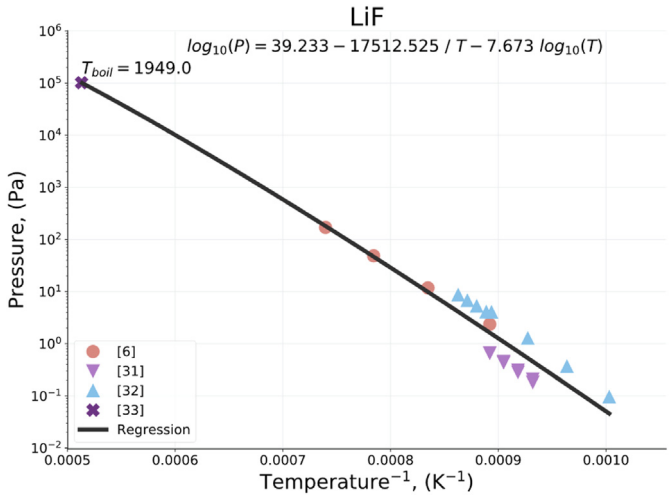

Fig. 7. Fit for LiF pure compound vapor pressure.

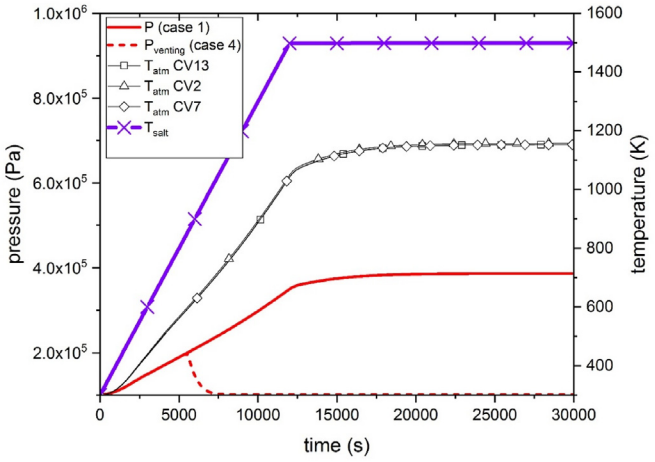

Fig. 8. Temperature of the salt and confinement atmosphere and the confinement pressure in the simulations.

section.

Fig. 8 shows the pressure of the confinement in cases 1 (similar to 2 and 3) and 4. In case 1, the pressure rises during the salt heat-up phase and reaches its maximum value of 0.385 MPa at approximately 15′000 s. Depressurization takes place in simulation case 4 at approximately 5000 s when the confinement pressure reaches 0.1 MPa over-pressure and decreases by venting to atmospheric pressure. Consequently, the average mass transfer coefficient of steam at the salt surface increases due to the increase in the flow velocity right after the venting was commenced. After the end of the salt heat up after 15′000 s, k_{st} stays in higher value compared to case 1, due to the decrease in gas density (Eqs. (5) and (6)), as shown in Fig. 9.

The parameters discussed above affect the calculation of the salt evaporation (Eqs. (1)–(9)). Overall, the thermal-hydraulic conditions in the presented simulations are largely dependent on the geometry of the salt confinement. This study considered only a generic design of a confinement, and thus more precise modeling will be needed once the final design of the MSFR is available. However, regardless if the precise geometry is in use, the results of the evaporation behavior of the salt and FP compounds presented below will serve to enlighten the mechanisms of fission product release from the salt.

3.5. FP and salt compound release

3.5.1. Fission products

Fig. 10 shows the released masses of fission products species CsI, CsF, I and LiI in cases 1 and 2 and the I_2 behavior in case 3. When I_2 was considered in the pure compound simulation case 3, it is immediately evaporated due to its high vapor pressure, resulting on CsI and LiI not being formed at all (Fig. 10b). If iodine stays unmixed in the salt, it will form molecular I_2 which will evaporate most

Table 4
Simulation matrix for the evaporation simulations.

	Case 1 (coupled)	Case 2 (pure compound VP)	Case 3 (pure compound VP + I_2)	Case 4 (coupled + venting)
Species considered in the evaporation simulation:	CsI, CsF, LiI, ThF_3 ThF_4, UF_4, UF_3, LiF, Li_2F_2, Li_3F_3, Li, I	CsI, CsF, LiI, ThF_4, UF_4, UF_3, LiF, Li_2F_2, Li_3F_3, Li	CsI, CsF, LiI, ThF_4, UF_4, UF_3, LiF, Li_2F_2, Li_3F_3, Li, I_2	CsI, CsF, LiI, ThF_3 ThF_4, UF_4, UF_3, LiF, Li_2F_2, Li_3F_3, Li, I
VPs from GEMS coupling	x			x
Venting of the confinement				x

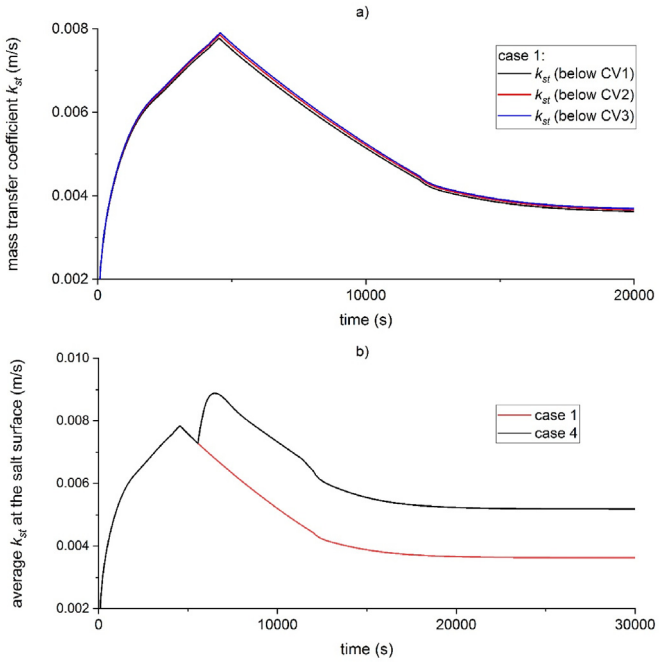

Fig. 9. a) Mass transfer coefficients of steam k_{st} at the salt surface in simulation case 1, b) average k_{st} in cases 1 and 4, i.e., without and with venting.

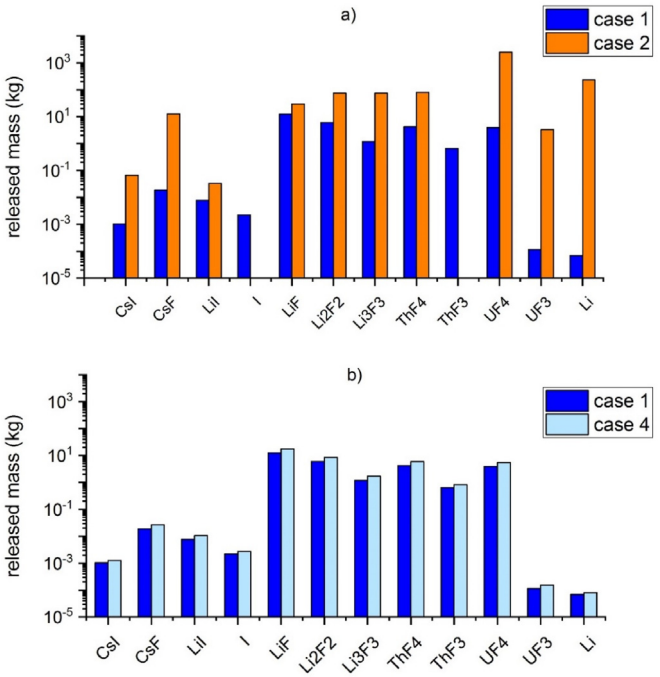

Fig. 11. Comparison of integral release from the salt after 30′000 s of simulation.

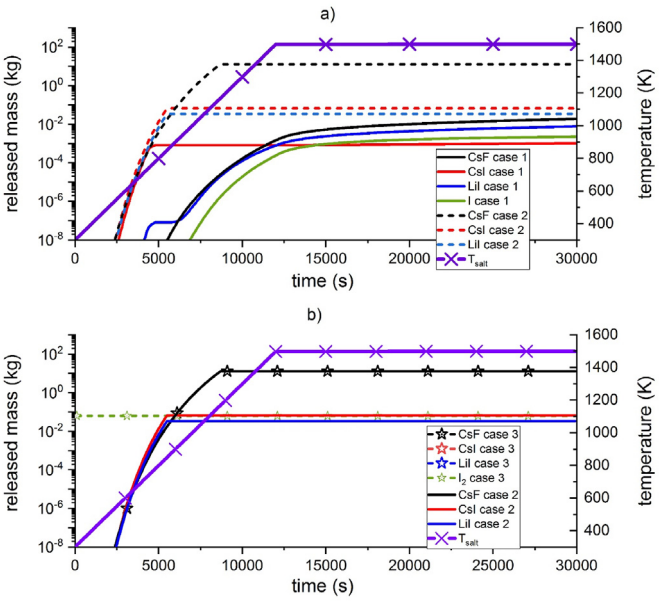

Fig. 10. Comparison of FPs released between a) case 1 and b) case 2 and case 3.

probably even before salt over heated in the accident conditions, as the normal operation temperature of the MSFR fuel is estimated to be 900–1000 K. If the fuel salt has excess F, formation of volatile I_2 is also possible, as described in section 3.1 (see iodine vapor pressures in Fig. 6). This result shows the importance of the speciation of iodine in the FP release simulations. At accident conditions, the behavior of I_2 in comparison to CsI or LiI in the confinement atmosphere would be very different, as molecular iodine would stay in vapor phase even at low temperatures and CsI and LiI would condense to form aerosols as the temperature decreases.

When assuming in case 2 that I_2 is not formed in the salt, evaporation of LiI and CsI can be investigated. CsI starts to evaporate in both cases 1 and 2 approximately at the same time. This is caused by the high vapor pressure of CsI below the temperature approximately 600 K, present in both coupled and uncoupled simulations. In the coupled simulation, CsI is not forming any intermediate compounds with Th or Li and is not involved in the formation of any solid solutions. Therefore, CsI behaves as a pure compound up until it melts and mixes with a liquid Li–Th–F phase. At approximately 700 K, CsI undergoes a phase transition to liquid, which shows as a rapid drop of its vapor pressure in Fig. 5. In earlier work by Capelli et al. [7], CsI has been shown to have a low solubility in liquid Li–Th–F phase, caused by a low excess (mixing) Gibbs energy between CsI and the components of the fluoride solution. Thus, only the ideal mixing effects are responsible for the drop in the CsI vapor pressure, observed in this work, after melting and mixing with the liquid Li–Th–F phase.

In case 2 simulation, CsI, CsF and LiI start to evaporate almost simultaneously due to their similar pure compound vapor pressures at this temperature range. Once the iodine is depleted from the salt, CsI and LiI release in case 2 stops at approximately 5′500 s, leading to a slightly higher total released mass of CsI. CsF release continues until all cesium has been released from the salt at approximately 8′700 s.

In the coupled simulation case 1, the behavior of CsF, CsI and LiI differs significantly compared to the pure compound simulations. After the phase transfer to liquid, LiI becomes the most volatile iodine containing species (the phase transition caused the “shoulder” in LiI mass at t = 5′000 s, shown in Fig. 10a), and its total evaporated mass eventually surpasses that of CsI at t = 11′500 s when the salt has already reached its maximum temperature 1500 K (Fig. 10). Additionally, at the end of the simulation at 30′000 s only 20% of the iodine was released from the salt. Similar behavior is also observed for CsF, where 1 mg of CsF has been released at approximately 7′500 s simulation time and at the end of the simulation at 30′000 s more than 99% of the Cs remains in the salt. Additionally for CsF, the onset of evaporation is significantly

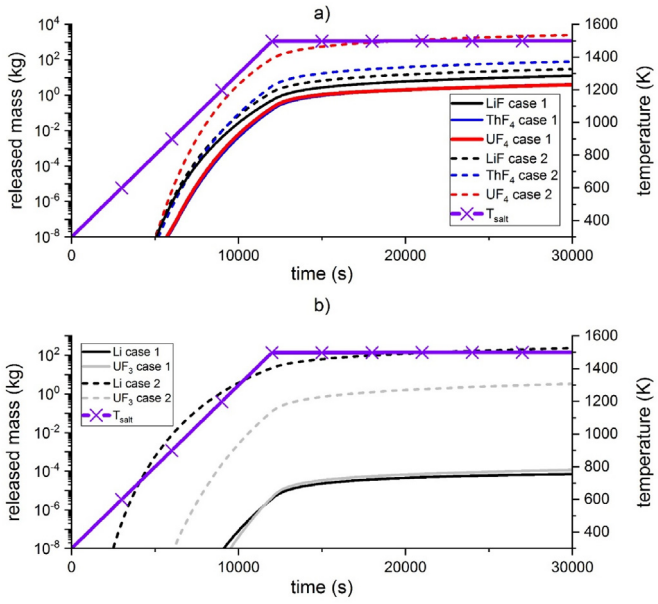

Fig. 12. Comparison of salt species behavior in cases 1 and 2.

delayed in simulation case 1 compared to case 2, due to its better retention in the salt mixture at temperatures below the melting point of the salt mixture, caused by formation of intermediate Cs–Li–Th–F compounds (mainly $CsTh_3F_{13}$).

The above results show that for both cesium and iodine, the retention in the salt is significantly increased when the mixing effects in the salt are considered. This can be seen clearly in Fig. 11a, where the integral release of compounds after 30′000 s simulation time in cases 1 and 2 is depicted. Additionally, Fig. 11a shows that the total amount of the most non-volatile compounds (Li and UF_3) released during the simulations remained very low (less than 1 g after 30′000 s of simulation time), which suggest that the vapor pressure cut-off limit of 10^{-8} Pa, which was used when selecting the species to be modeled, was justified.

3.5.2. Salt species

Fig. 12 shows the evaporation behavior of salt species in simulation cases 1 and 2. For the LiF, UF_4 and ThF_4 species, the onset of evaporation was not considerably varied between the pure compound and salt mixing simulations but takes place in both at approximately 5′000–6′000 s. The largest difference in the timing of the release was seen in the species Li and UF_3 whose release ended up being delayed in the coupled simulation approximately 7′000 s and 3′000 s, respectively. This is caused by a much higher activity of pure Li compared to it being mixed in the fuel salt with other salt and FP compounds. Additionally, uncertainties in the pure compound vapor pressure of UF_3, found from the literature [37,38] can play a role in the significant difference seen in the results from cases 1 and 2.

Overall, similar to FPs Cs and I, almost all the salt species were observed to be retained better in the fuel salt when salt mixing was considered and the coupled simulation method was used, compared to the pure compound simulation, which is clearly observed in the integral release at 30′000 s, shown in Fig. 11a. Additionally, in the coupled simulations (case 1) LiF was found to be the most volatile of the salt components, whereas in case 2 several species like ThF_4, UF_4 and Li contributed more to the overall mass release. This indicates that in addition to the evaporation of the fission products, the salt mixing effects are also important when considering the realistic modeling of the evaporation of the actinide compounds.

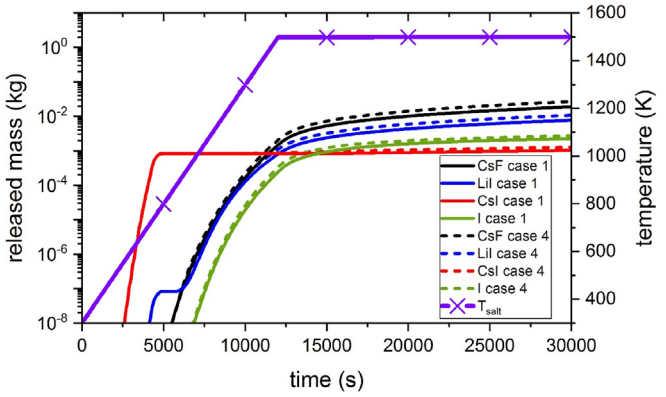

Fig. 13. Fission product release in case 1 and case 4.

3.5.3. Effect of venting

The change in the atmospheric pressure has almost no effect on the timing of the FP and salt material release, which is seen by comparing cases 1 and 4 in Fig. 13. The only difference between these two cases was the reduction of the confinement pressure by venting in case 4 at time = 5000 s. The decreased pressure (and in a short period during the pressure drop the increased flow velocity in the confinement) increased the mass transfer coefficient at the salt surface, as discussed in the previous section (see Fig. 9), which resulted in a slight increase in the evaporation rates of all species considered in the simulations. Thus, the main result of the confinement depressurization was that the overall released amount of FPs and salt components was slightly increased in lower atmospheric pressure in the venting case, as is shown in Fig. 11b.

The results of this analysis show that if the depressurization of the confinement becomes inevitable, the increase in the evaporated mass and the timing of the evaporation of different FP and salt materials need to be taken into account when venting strategies of the MSR confinement are being designed. In order to determine the speciation of the material reaching the filtration system outside the confinement and eventually the environment, more detailed simulations of the source term need to be performed.

4. Conclusions

In this study, the evaporation of fission products and salt compounds from the MSR fuel under accident conditions was investigated. A comparison was done between different models, considering either evaporation of pure compounds from a confinement surface or evaporation of FP and salt species from a fuel salt mixture. Additionally, the effect of the confinement building pressure reduction by venting on the evaporation process was addressed. The conclusions can be summarized as follows:

- The release of FPs and salt materials was reduced when the salt mixing was considered in the coupled simulation model, compared to the pure compound simulations. Additionally, the timing of the release of different compounds is determined by the mixing effects in the salt.
- Depressurization affects the mass transfer coefficient at the salt surface, increasing the amount of evaporated materials.
- Thermodynamic modeling of the salt mixture plays a crucial role in determining the dominant volatile species that need to be considered when evaporation of the salt is investigated. This

shows that the simplified evaporation modeling using the pure compound vapor pressures is not sufficient, especially in the case of the MSRs, where chemical reactions in the liquid salt are important. Additionally, vapor phase iodine speciation is greatly affected by the amount of F in the salt mixture. This could have a significant effect on the FP behavior during salt evaporation and needs to be more comprehensively studied in the future.
- Additionally, it is important to note that the operating temperature of an MSR is high, possibly between 900 and 1000 K. Many of the species considered in this study were seen to evaporate at this temperature range. This should be taken into account in the investigation of the salt and FP behavior in the primary circuit of the reactor also during normal operation.

5. Future work

The possible future improvements to the study could include:

- In addition to Cs and I, more fission product elements should be added to the simulations. This will require more experimental information about the FP and salt mixtures, which can be used for the validation of the thermodynamic modeling. Potential FPs could include for example Ba, which is known to be volatile in reducing atmosphere in LWR severe accident conditions [53] and Cd, that could affect the I speciation through the formation of CdI_2 [54]
- Only a crude preliminary design of the salt confinement was used in this study. More precise model of the confinement geometry and the accident sequences in the MSFR are needed to determine the importance of the thermal-hydraulic conditions to the source term. With the improved confinement modeling, the transport and deposition of active particles and vapors could also be more accurately taken into account.
- Possible effects of the under and over fluorination should be considered more thoroughly. Additionally, the effects of variations of fluorine concentration in the salt for FP volatility during the reactor operation could be further considered.
- In these simulations, the salt was considered to be homogenous without any consideration of the physical modeling of the liquid salt. More sophisticated modeling of the salt could cover heterogeneity of the salt and heat and mass transfer in the liquid phase. Additionally, more detailed model of the salt heating by the decay heat could be covered in the future work.
- Coupling of the burnup calculation with the thermodynamic assessment of each species volatility, e.g. presence on I_2 in off-gas system could be considered.

Declaration of competing interest

The authors declare that they have no known competing financial interests or personal relationships that could have appeared to influence the work reported in this paper.

CRediT authorship contribution statement

Jarmo Kalilainen: Conceptualization, Methodology, Investigation, Visualization, Data curation, Writing - original draft. **Sergii Nichenko:** Conceptualization, Methodology, Software, Investigation, Visualization, Writing - review & editing. **Jiri Krepel:** Conceptualization, Methodology, Data curation, Visualization, Writing - review & editing, Project administration, Funding acquisition.

Acknowledgements

This work has received funding from the Euratom research and training programme 2019–2023 under grant agreement No 847527. The authors would like to thank Dr. Terttaliisa Lind for her valuable comments in preparation of this manuscript.

All raw/processed data required to reproduce these findings cannot be shared at this time due to time limitations but can be made available from the corresponding author on reasonable request.

Appendix. list of species considered in the thermodynamic simulation

Solid	Liquid	Gaseous
Li_7ThUF(ss)	CsF(l)	Cs(g)
$LiThU_4F_{17}$(ss)	CsI(l)	Cs_2(g)
$ThUF_4$(ss)	LiF(l)	Cs_2F_2(g)
C	LiI(l)	CsF(g)
CsF	ThF_4(l)	Cs_2I_2(g)
CsI	ThI_4(l)	CsI(g)
$Cs_2Th_3F_{14}$	UF_3(l)	CsLi(g)
Cs_2ThF_6	UF_4(l)	F(g)
Cs_3ThF_7		F_2(g)
$CsTh_2F_9$		I(g)
$CsTh_3F_{13}$		I_2(g)
$CsTh_6F_{25}$		Li(g)
α-CsThF5		Li_2F_2(g)
Cs_2ThI_6		Li_3F_3(g)
I_2		LiF(g)
Li		Li_2I_2(g)
$LiCsF_2$		Li_3I_3(g)
LiF		LiI(g)
LiI		Th(g)
Li_2O		ThF_2(g)
Li_3ThI_7		ThF_3(g)
$Li_7Th_6F_{31}$		ThF_4(g)
$LiTh_4F_{17}$		ThI(g)
Li_3ThI_7		ThI_2(g)
$LiTh_2I_9$		ThI_3(g)
$LiTh_4I_{17}$		ThI_4(g)
$LiThI_5$		U(g)
Li_4UF_8		UF(g)
$Li_7U_6F_{31}$		UF_2(g)
LiU_4F_{17}		UF_3(g)
Th		UF_4(g)
ThF_4		UI(g)
ThI		UI_2(g)
ThI_2		UI_3(g)
ThI_3		UI_4(g)
ThI_4		
U		
U_2F_9		
U_4F_{17}		
UF_3		
UF_4		
UI_3		
UI_4		

* (ss) solid solution, (g) gas (l) liquid.

References

[1] J. Serp, M. Allibert, O. Beneš, S. Delpech, O. Feynberg, V. Ghetta, D. Heuer, D. Holcomb, V. Ignatiev, J.-L. Kloosterman, L. Luzzi, E. Merle-Lucotte, J. Uhlir, R. Yoshioka, D. Zhimin, The molten salt reactor (MSR) in generation IV: overview and perspectives, Prog. Nucl. Energy 77 (2014), 308-219.

[2] MELCOR computer code manuals vol. 2: reference manual, in: Sandia National Laboratories, United States of America, Albuquerque, NM, 2017. Version

2.2.9541.
[3] G. Brillant, C. Marchetto, W. Plumecocq, Fission product release from nuclear fuel I. Physical modelling in the ASTEC code, Ann. Nucl. Energy 61 (2013) 88–95.
[4] E. Compere, S. Kirslis, E. Bohlmann, F. Blankenship, W. Grimes, Fission Product Behavior in the Molten Salt Reactor Experiment. ORNL-4865, Oak Ridge National Laboratory, Oak Ridge, United States of America, 1975.
[5] N. Vozarova, Behaviour of Fission Products in the Molten Salt Reactor Fuel, MSc thesis, ETH Zürich, Switzerland, 2016.
[6] E. Capelli, O. Beneš, J.-Y. Colle, R. Konings, Determination of the thermodynamic activities of LiF and ThF in the LixTh1-xF4-3x liquid solution by Knudsen effusion mass spectrometry, Phys. Chem. Chem. Phys. 17 (2015) 30110.
[7] E. Capelli, O. Beneš, R. Konings, Thermodynamics of soluble fission products cesium and iodine in the Molten Salt Reactor, J. Nucl. Mater. 501 (2018) 238–252.
[8] M. Taira, Y. Arita, M. Yamawaki, The evaporation behavior of volatile fission products in FLiNaK salt, Open Access J. Sci. Technol. 5 (2017). ID 101315.
[9] Y. Sekiguchi, K. Uozumi, T. Koyama, T. Terai, Fundamental study on the vaporization of cesium and iodine dissolved in LiF-NaF-KF molten salt, J. Nucl. Mater. 522 (2019) 136–143.
[10] A.L. Wright, NUREG/CR-6193, Primary Circuit Fission Product Release and Transport, Oak Ridge National Laboratory, Oak Ridge, United States of America, 1994.
[11] S. Wang, M. Massone, A. Rineiski, E. Merle-Lucotte, A. Laureau, D. Gérardin, D. Heuer, M. Allibert, A passive decay heat removal system for emergency draining tanks of molten salt reactors, Nucl. Eng. Des. 341 (2019) 423–431.
[12] S. Beils, "Overview of the safety analysis of the MSFR. Present. SAMOFAR Final Meet., July 4th, 2019," [Online]. Available: http://samofar.eu/wp-content/uploads/2019/07/SAMOFAR_FinalMeeting_04.07.2019_WP1_Beils.pdf. [Accessed 17. 9. 2019].
[13] B. Hombourger, Conceptual Design of a Sustainable Waste-Burning Molten Salt Reactor. PhD Thesis, Ecole Polytechnique Federale de Lausanne, Lausanne, Switzerland, 2018.
[14] B. Hombourger, J. Křepel and A. Pautz, "The EQL0D procedure for fuel cycle studies in molten salt reactors and its application to the transition to equilibrium of selected designs," Accepted by Ann. Nucl. Energy.
[15] J. Leppänen, M. Pusa, T. Viitanen, V. Valtavirta, T. Kaltiaisenaho, The Serpent Monte Carlo code: status, development and applications in 2013, in: Ann. Nucl. Energy, Joint International Conference on Supercomputing in Nuclear Applications and Monte Carlo 2013, SNA + MC 2013. Pluri- and Trans-disciplinarity, Towards New Modeling and Numerical Simulation Paradigms, vol. 82, 2015, pp. 142–150.
[16] M. Pusa, J. Leppänen, Solving linear systems with sparse Gaussian elimination in the Chebyshev rational approximation method, Nucl. Sci. Eng. 175 (2013) 250–258.
[17] M. Allibert, D. Gerardin, D. Hauer, E. Huffer, A. LAureau, E. Merle, S. Beils, A. Cammi, B. Carluec, S. Delpech, A. Gerber, E. Girardi, J. Krepel, D. Lathouwers, D. Lecarpentier, S. Lorenzi, L. Luzzi, S. Poumerouly, M. Ricotti, Tiberi, Description of initial reference design and identification of safety aspects.," SAMOFAR (A paradigm shift in nuclear reactor safety with the molten salt fast reactor), Eur. Project (2016). Work-Package WP1, Deliverable D1.1, Grant Agreement number: 661891.
[18] J. Krepel, V. Sisl, S. Nichenko, B. Hombourger, Transition to closed Th-U fuel cycle in fluoride salts based MSR, in: ICAPP 2019 - International Congress of Advances in Nuclear Power Plants, 2019. Juan-les-pins, France.
[19] J. Welty, C. Wicks, R. Wilson, G. Rorrer, Fundamentals of Momentum Heat, and Mass Transfer, fourth ed., John Wiley & Sons, 2000.
[20] R.B. Bird, W.E. Stewart, E.N. Lightfoot, Transport Phenomena, second ed., John Wiley & Sons Inc., New York, Unites States, 2002.
[21] P. Woskov, S. Sundaram, W. Daniel Jr., D. Miller, Molten salt dynamics in glass melts using millimeter-wave emissivity measurements, J. Non-Cryst. Solids 341 (2004) 21–25.
[22] GEMS, "GEM Software (GEMS) Home," Paul Scherrer Institut [Online]. Available, http://gems.web.psi.ch. (Accessed 28 January 2020).
[23] G. Miron, D. Kulik, S. Dmytrieva, T. Wagner, GEMSFITS: code package for optimization of geochemical model parameters and inverse modeling, Appl. Geochem. 55 (2015) 28–45.
[24] N. Shcherbina, N. Kivel, I. Günther-Leopold, D. Kulik, J. Bertsch, HERACLES project and thermodynamic database homepage [Online]. Available, http://www.psi.ch/heracles/, 2012. (Accessed 18 October 2019).
[25] SACSESS, EU FP7 Project SACSESS: Safety of ACtinide separation processes [Online]. Available, http://www.sacsess.eu/, 2015. (Accessed 10 September 2019).
[26] P. Glynn, Solid solution solubilities and thermodynamics: sulfates, carbonates and halides, Rev. Mineral. Geochem. 40 (2000) 481–511.
[27] E. Capelli, O. Beneš, M. Beilmann, R.J.M. Konings, Thermodynamic investigation of the LiF–ThF4 system, J. Chem. Therm. 58 (2013) 110–116.
[28] A.D. Pelton, P. Chartrand, G. Eriksson, The modified quasi-chemical model: Part IV. Two-sublattice quadruplet approximation, Metall. Mater. Trans. 32 (6) (2001) 1409–1416.
[29] E. Capelli, O. Beneš, R. Konings, Thermodynamic assessment of the LiF–NaF–BeF2–ThF4–UF4 system, J. Nucl. Mat., Bd. 449 (2014) 111–121.
[30] H. Huang, W. Wang, Q. Yuan, X. Rao, Y. Jing, G. Yi, L. Luo, Y. Liu, Pressure-dependence of mechanical and thermodynamic properties of Al3Zr in Al–Li alloys from first-principles calculations, Phil. Mag. 99 (8) (2019) 971–991.
[31] L. Lugo, M.J.P. Comuñas, E.R. López, J. García, J. Fernández, Pressure and temperature dependence of the excess thermodynamic properties of binary dimethyl carbonate + n-octane mixtures, Can. J. Chem. 81 (7) (2003) 840–849.
[32] A. Abdollahi, S.M. Gholzan, Pressure–temperature dependence of thermodynamic properties of ScAlO 3 perovskite from first principles, Int. J. Thermophys. 36 (8) (2015) 2273–2282.
[33] D. Lide, CRC Handbook of Chemistry and Physics, CRC Press, Boca Raton, FL, 2005.
[34] R. Scheffee, J. Margrave, Vapor pressure equations for species over solid and liquid LiF, J. Chem. Phys. 31 (1959) 1682.
[35] D. Hildenbrand, W. Hall, F. Ju, N. Potter, Vapor pressures and vapor thermodynamic properties of some lithium and magnesium halides, J. Cehm. Phys. 40 (1964) 2882.
[36] P. Patnaik, Handbook of Inorganic Chemicals, United States of America: McGraw-Hill Companies, Inc., New York, 2003. Ny 10121-2298.
[37] K. Roy, V. Rajendra Prasad, V.Z.S.S.D. Venugopal, Studies on (2UF4+H2 = 2UF3+2HF) and vapour pressure of UF3, J. Chem. Therm. 14 (1982) 389–394.
[38] L. Gorokhov, V. Smirnov, Y. Khodeev, Thermochemical characteristics of uranium fluoride UFn molecules, Russ. J. Phys. Chem. 58 (1984) 980–983.
[39] A. Tosolin, O. Beneš, J.-Y. Colle, P. Soucek, L. Luzzi, R. Konings, Vaporization behaviour of the molten salt fast reactor fuel: the LiF-ThF4-UF4 system, J. Nucl. Mater. 508 (2018) 319–328.
[40] N. Nagarajen, M. Bhupathy, R. Prasad, Z. Singh, V. Venugopal, D. Sood, Vaporization behavior of uranium tetrafluoride, J. Chem. Thermodyn. 12 (1980) 329–333.
[41] S. Langer, F. Blankenship, The vapour pressure of uranium tetrafluoride, J. Inorg. Nucl. Chem. 14 (1960) 26–31.
[42] R. Thoma, B. Sturm, E. Guinn, Molten-salt Solvents for Fluoride Volatility Processing of Aluminum-Matrix Nuclear Fuel Elements, Oak Ridge National Laboratory, Oak Ridge, United States of America, 1964. ORNL-3594.
[43] A. Darnell, F. Keneshea, Vapor pressure of thorium tetrafluoride, J. Phys. Chem. 62 (1958) 1143–1145.
[44] K. Lau, R. Brittain, D. Hilderbrand, High temperature thermodynamic studies of some gaseous thorium fluorides, J. Chem. Phys. 90 (1989) 1158.
[45] N. Nagarajen, M. Bhupathy, R. Prasad, Z. Singh, V. Venugopal, D. Sood, Vaporization thermodynamics of thorium tetrafluoride, Thermochim. Acta 36 (1980) 85–89.
[46] E. Cordfunke, Thermodynamic properties of CsI. II. Vapour pressures and thermochemical properties of CsI(g) and Cs2I2(g), Thermochim. Acta 108 (1986) 45–55.
[47] G. Janz, Molten Salts Handbook, Academic press Inc., New York, 1967.
[48] M. Scheer, J. Fine, Entropies, heats of sublimation, and dissociation energies of the cesium halides, J. Chem. Phys. 36 (6) (1962) 1647–1653.
[49] M. Eisenstadt, G. Rothberg, P. Kusch, Molecular composition of alkali fluoride vapors, J. Chem. Phys. 29 (4) (1958) 797–804.
[50] N. Vozarova, A. Smith, J.-Y. Colle, P. Raison, D. Douexiere, R. Konings, O. Benes, Thermodynamic determination and assessment of the CsF-ThF4 system, J. Chem. Thermodyn. 114 (2017) 71–82.
[51] L. Bencze, A. Lesar, A. Popovic, The evaporation thermodynamics of lithium iodide. Mass spectrometric and ab initio studies, Rapid Commun. Mass Sprectrom. 12 (1998) 917–930.
[52] M. Berkenblit, A. Reisman, The vapor pressure of iodine in the temperature interval 43-80C, J. Electrochem. Soc. 113 (1) (1966) 93–95.
[53] Y. Pontillon, G. Ducros, Behaviour of fission products under severe PWR accident conditions. The VERCORS experimental programme—Part 3: release of low-volatile fission products and actinides, Nucl. Eng. Des. 240 (2010) 1867–1881.
[54] N. Girault, C. Fiche, A. Bujan, J. Dienstbier, Towards a better understanding of iodine chemistry in RCS of nuclear reactors, Nucl. Eng. Des. 239 (6) (2009) 1162–1170.